1 **Enzymatic dissociation induces transcriptional and proteotype bias in brain cell populations**

2

3 Daniele Mattei[1,8 #,*], Andranik Ivanov[2,#,*], Marc van Oostrum[3,#], Stanislav Pantelyushin[4,#], Juliet

4 Richetto[1,5], Flavia Mueller[1], Michal Matheus Beffinger,[4] Linda Schellhammer [4], Johannes vom

5 Berg[4], Bernd Wollscheid[3], Dieter Beule[2,6], Rosa Chiara Paolicelli[7,§], Urs Meyer [1,5,§].

6

7 [1]Institute of Pharmacology and Toxicology, University of Zurich-Vetsuisse, Zurich, Switzerland.

8 [2]Core Unit Bioinformatics, Berlin Institute of Health, Berlin, Germany; Charité-

9 Universitaetsmedizin, Berlin, Germany.

10 [3]Institute of Molecular Systems Biology and Department for Health Sciences and Technology, ETH

11 Zürich, Zurich, Switzerland.

12 [4]Institute of Laboratory Animal Science, University of Zurich, Schlieren, Switzerland.

13 [5]Neuroscience Centre Zurich, University of Zurich and ETH Zurich, Zurich, Switzerland.

14 [6]Max Delbrück Center for Molecular Medicine in the Helmholtz Association (MDC), Berlin,

15 Germany.

16 [7]Department of Biomedical Sciences, University of Lausanne, Rue du Bugnon 7, 1005 Lausanne,

17 Switzerland.

18 [8]Lead Contact.

19 [#]Equal contributors.

20 [§]Joint senior authors.

21

22 *Correspondence: Daniele Mattei, Ph.D., Institute of Pharmacology and Toxicology, University of
23 Zurich-Vetsuisse, Winterthurerstrasse 260, 8057 Zurich, Switzerland; Tel: +41 44 635 88 44, Email:
24 daniele.mattei@vetpharm.uzh.ch; Andranik Ivanov, PhD, Core Unit Bioinformatics, Berlin Institute
25 of Health, Invalidenstrasse 80, 10117, Berlin, Germany; Tel: +49 30 450543608, Email:
26 andranik.ivanov@bihealth.de

27
28

1 **Abstract**

2

3 Different cell isolation techniques exist for transcriptomic and proteotype profiling of brain cells.

4 Here, we provide a systematic investigation of the influence of different cell isolation protocols on

5 transcriptional and proteotype profiles in mouse brain tissue by taking into account single-cell

6 transcriptomics of brain cells, proteotypes of microglia and astrocytes, and flow cytometric analysis

7 of microglia. We show that standard enzymatic digestion of brain tissue at 37°C induces profound

8 and consistent alterations in the transcriptome and proteotype of neuronal and glial cells, as compared

9 to an optimized mechanical dissociation protocol at 4°C. These findings emphasize the risk of

10 introducing technical biases and biological artefacts when implementing enzymatic digestion-based

11 isolation methods for brain cell analyses.

12 **Key Words:** Microglia, Astrocytes, Transcriptomics, Proteotype, Brain Tissue, Dissociation

13

14

15

16

1 **Introduction**

2 The neuroscience field is constantly implementing novel techniques for gene sequencing, epigenetic

3 analyses and proteotype profiling at a rapidly increasing rate. Obtaining single cell suspensions from

4 intact brain tissue is essential for downstream cell specific transcriptomic and proteotype analyses.

5 The main techniques available to obtain single cell suspensions from brain tissue are enzymatic

6 digestion (ED) and mechanical dissociation (MD). The latter is typically carried out at 4°C (Mattei

7 et al., 2017), whereas ED requires incubation at temperatures between 30-37°C (Saunders et al.,

8 2018; Tiklova et al., 2019; Zhang et al., 2014). With both techniques, cells such as neurons and

9 microglia will lose their processes and suffer harsh conditions whereby a proportion of cells die

10 during the dissociation process. Although loss of cells and of their processes is likely to introduce

11 technical artefacts in both cases, we hypothesize that at warm temperatures, as opposed to 4°C,

12 surviving cells may overreact to the non-physiological milieu containing shredded extracellular

13 matrix, cell debris, and cytoplasmic leakage (Reichard & Asosingh, 2019). Furthermore, the ED

14 technique is associated with marked temperature shifts occurring between the eventual cell isolation

15 step and the preceding perfusion which is typically carried out at cold temperatures to remove blood

16 contamination from the brain. Thermal shocks resulting from temperature shifts have been shown to

17 elicit widespread transcriptional changes, even within short time windows (Mahat, Salamanca,

18 Duarte, Danko, & Lis, 2016). Hence, unlike MD at cold temperatures, which largely spares the

19 cellular transcriptome and proteome (Fujita, 1999), the ED technique may introduce additional

20 biological biases to the transcriptional and proteotype profiles of cells.

21 A few studies have thus far warned for possible ED-induced artefacts, but not as a main focus

22 of investigation, and proposed the use of transcriptional/translational blockers to prevent *de novo*

23 transcription/translation (Ayata et al., 2018; Hrvatin et al., 2018; Wu, Pan, Zuo, Li, & Hong, 2017).

24 Nevertheless, this issue has only been considered for transcriptional analyses, whereby possible

25 biological consequences of ED on the proteotype profiling (e.g. flow cytometry and mass-

26 spectrometry analyses) has up to today not been taken into consideration. Importantly, the use of

27 transcription/translation inhibitors do not prevent biological downregulation of RNAs and proteins

28 that might occur during ED, nor can they prevent unwanted alterations in epigenetic marks or

1 internalization/externalization of receptors which might be crucial readouts for certain cell specific

2 analyses. Given that at present, ED is the most widely used method to obtain single cell suspensions

3 from brain tissue (Figure S1), it is pivotal to understand the extent of cell responses when exposed

4 to ED as compared to a method which holds cells in a quiescent state. We here investigate

5 systematically the influence of different cell isolation protocols on transcriptional and proteotype

6 profiles in mouse brain tissue, by taking into account single-cell transcriptomics, proteotypes of

7 microglia and astrocytes, and flow cytometric analysis of microglia. By comparing the transcriptional

8 and proteotype profiles of brain cells isolated via ED at 37°C and via MD at 4°C, our study provides

9 a comprehensive transcriptomic and proteotype resource that can be used to identify and correct for

10 artefacts in previously published data sets generated via ED. Furthermore, with the present work, we

11 share an optimized and easy-to-establish MD protocol at 4°C, which is cost effective and technically

12 easier to implement than conventional ED-based protocols.

13

Material and Methods

Animals

16 Nine to ten weeks old male C57BL6/N mice (Charles River Laboratories, Sulzfeld, Germany) were

17 used throughout the study. They were caged 3-5 animals per cage in individually ventilated cages

18 (IVCs). The animal vivarium was a specific-pathogen-free (SPF) holding room, which was

19 temperature- and humidity-controlled (21 ± 3 °C, $50 \pm 10\%$) and kept under a reversed light–dark

20 cycle (lights off: 09:00 AM–09.00 PM). All animals had ad libitum access to the same food (Kliba

21 3436, Kaiseraugst, Switzerland) and water throughout the entire study. All procedures described in

22 the present study had been previously approved by the Cantonal Veterinarian's Office of Zurich, and

23 all efforts were made to minimize the number of animals used and their suffering.

24 For the glioma model, six to eight weeks old C57BL/6JRj male mice (Janvier Labs, Le Genest-Saint-

25 Isle, France) were used for the inoculation of the GL-261 brain tumor cell line. They were caged 3-

26 5 animals per cage in individually ventilated cages (IVCs). The animal vivarium was a specific-

27 pathogen-free (SPF) holding room, which was temperature- and humidity-controlled (21 ± 3 °C,

28 $50 \pm 10\%$). All animals had ad libitum access to the same food and water throughout the entire study.

4

1   All procedures described in the present study had been previously approved by the Cantonal

2   Veterinarian's Office of Zurich (License 246/2015), and all efforts were made to minimize the

3   number of animals used and their suffering.Briefly, a total of 20'000 cells in 2 μL PBS were injected

4   at a speed of 1 μL/min intracranially into mice using a neurostar stereotaxic robot as described in

5   Beffinger et al. 2019 (Beffinger, Schellhammer, Pantelyushin, & Vom Berg, 2019).

6   **GL-261luc cells**

7   The murine GL-261 brain tumor cell line (syngenic to C57BL/6), was stably transfected with pGl3-

8   ctrl and pGK- Puro (Promega) and selected with puromycin (Sigma-Aldrich) to generate luciferase-

9   stable GL-261 cells. Cells were cultured at 37°C 5% CO_2 in DMEM supplemented with 10% heat

10 inactivated fetal calf serum, 1% L-glutamine (Thermo Fisher Scientific) and 1% Pen-Strep (Sigma).

11 **Surgical procedures**

12 For glioma inoculation, 6-10 weeks old mice were anesthetized using a mixture of fentanyl

13 (Helvepharm AG), midazolam (Roche Pharma AG) and medetomidin (Orion Pharma AG). GL261

14 cells were injected intracranially (i. c.) in the right hemisphere using a stereotactic robot (Neurostar).

15 Briefly, a blunt-ended syringe (Hamilton; 75N, 26s/2"/2, 5 μl) was placed 1.5 mm lateral and 1 mm

16 frontal of bregma. The needle was lowered into the burr hole to a depth of 4 mm below the dura

17 surface and retracted 1 mm to form a small reservoir. Injection was performed in a volume of 2 μl at

18 1 μl/min. After leaving the needle in place for 2 min, it was retracted at 1 mm/min. The burr hole

19 was closed with bone wax (Aesculap, Braun) and the scalp wound was sealed with tissue glue

20 (Indermil, Henkel). Anesthesia was interrupted using a mixture of flumazenil (Labatec Pharma AG)

21 and Buprenorphine (Indivior Schweiz AG), followed by injection of atipamezol 20 minutes later

22 (Janssen). Carprofen (Pfizer AG) was used for perioperative analgesia. Mice were collected for

23 experiments at 20 days post glioma inoculation, and the tumor bearing hemispheres where processed

24 with either mechanical dissociation at 4°C or with enzymatic digestion at 37°C to test the respective

25 technique's efficiency in producing single cell suspensions for FACS analysis (see below).

26

27 **Brain Dissociation and Cell Isolation**

1   The protocol has been optimized from our previous protocol (Mattei et al., 2017) and from the

2   procedures provided by Miltenyi (adult brain dissociation kit, ABDK, Miltenyi). The protocol is

3   optimized for the dissociation and isolation of cells from brain tissue of small volume (e.g., mouse

4   hippocampi). A detailed dissociation protocol for larger pools of tissue or whole adult mouse brain

5   is provided in Additional File 1. A detailed list of materials and reagents recommended for the

6   following cell isolation protocol is displayed in Table 1 below.

7

8   **Table 1:** List of material and reagents for the cell isolation procedure.

Material	Product Code
20 ml Syringes, Bbraun	4606205V
23 G needles, 25 mm Sterican	4657667
Petri dishes, Thermo Fisher Scientific	11339283
5 ml Tubes, Eppendorf	0030119452
1x DPBS, Thermo Fisher Scientific	14190144
10x DPBS, Thermo Fisher Scientific	14200075
Percoll, GE Healthcare	17089101
1 ml Dounce Homogenizer, Active Motif	40401
Hibernate A, Brainbits	HAPR
70 μm cell strainers, Fisher Scientific	15370801
Collagenase, Sigma Aldrich/Merck	10269638001
DNase I, Sigma Aldrich/Merck	10104159001
RPMI medium, Sigma Life Science	R8758-500ml
MACS MS Columns, Miltenyi	130-042-201
CD11b magnetic beads, Miltenyi	130-093-634
ACSA-II magnetic beads, Miltenyi	130-097-678
7.5% BSA in PBS, Thermo Fisher Scientific	11500496
FBS, Thermo Fisher Scientific	26140087
Swing Bucket Centrifuge 5810, Eppendorf	5810000010

9

10   The animals were deeply anesthetized with an overdose of Nembutal (Abbott Laboratories, North

11   Chicago, IL, USA) and transcardially perfused with 15 ml ice-cold, calcium- and magnesium-free

12   Dulbecco's phosphate-buffered saline (DPBS, pH 7.3-7.4) via a 20 ml syringe and a 23 G needle (25

13   mm length). The brains were quickly removed and washed with ice-cold DPBS, after which the

14   hippocampi were dissected on a cooled petri dish and placed in ice-cold Hibernate-A medium.

15   For enzymatic digestion (ED) at 37°C, 2-4 hippocampi/sample were grossly minced with

16   surgical scissors and placed in a sterile 12-well plate containing dissection medium pre-heated to

17   37°C. The dissection medium contained Roswell Park Memorial Institute (RPMI) medium, 10% fetal

18   bovine serum (FBS), 0.4mg/ml collagenase and 2mg/ml DNaseI. The plate was then placed in a

1   standard cell culture incubator at 37°C with 95% O_2 and 5% CO_2 for a total of 30 minutes. After the

2   first 15 minutes of incubation, the tissue was mixed with a pipette to optimize the enzymatic

3   digestion. At the end of the 30 minutes enzymatic digestion, the plate was placed on ice, and the

4   digested tissue was transferred to a 1 ml Dounce homogenizer to complete the dissociation of

5   remaining tissue pieces (on ice). Thereafter, the homogenate was sieved through a 70 μm cell strainer

6   mounted onto a 50 ml Falcon tube and transferred into 5 ml Eppendorf tubes on ice. Eppendorf tubes

7   made of polypropylene were used because cells show less adherence to this material as opposed to

8   polystyrene (Reichard & Asosingh, 2019).

9   Mechanical dissociation (MD) at 4°C was carried out on ice, while all the solutions were kept

10   at 4°C. 2-4 hippocampi/sample were dissociated in 1.5 ml Hibernate-A medium in a 1 ml Dounce

11   homogenizer with a loose pestle. The 1 ml Dounce homogenizer used here (see Table 1) has enough

12   capacity for a volume of 1.5 ml, which is preferable for optimal tissue dissociation. Furthermore, this

13   mechanical homogenizer allows enough space between the glass pot and the loose pestle, which is

14   required for efficient tissue homogenization without extensive cell loss. The tissue was gently

15   dounced until no bigger tissue pieces were visible. The homogenized tissue was then sieved through

16   a 70μm cell strainer mounted onto a 50 ml Falcon tube. The Dounce homogenizer was then washed

17   twice with 1 ml Hibernate-A, whereby each wash is poured onto the cell strainer. The homogenized

18   hippocampi were then transferred to 5 ml Eppendorf tubes and kept on ice as described above.

19   After ED at 37°C or MD at 4°C, all samples were handled the same way and further processed

20   as follows:

21   The homogenates were pelleted at 400xg for 6 minutes at 4°C in a swing-bucket rotor centrifuge

22   (Eppendorf). The supernatants were removed and 1 ml ice-cold DPBS (pH 7.3-7.4) was added to all

23   samples. The pellets were then re-suspended with a P1000 micropipette, applying a pipette-tip cut-

24   off. After re-suspension, the final volume in each tube was brought to 1.5 ml. 500 μL of freshly

25   prepared isotonic percoll solution was then added to each sample (final volume: 2 ml) and mixed

26   well (applying a pipette-tip cut-off to optimize the mixing). Percoll was rendered isotonic by mixing

27   1 part of 10x calcium- and magnesium-free DPBS (pH 7.3-7.4) with 9-parts of percoll. Importantly,

28   the pH of percoll was adjusted to 7.3-7.4 with 5 molar hydrochloric acid before starting the isolation

1   procedure. The percoll solution was mixed properly with the cell suspension, after which 2 ml of

2   DPBS were gently layered on top of it with a pipette boy set on the slowest speed, creating two

3   separate layers. The samples were centrifuged for 10 minutes at 3000xg. The centrifugation resulted

4   in an upper layer consisting of DPBS and a lower layer consisting of percoll. The two layers were

5   separated by a disk of myelin and debris, while the cells were located at the bottom of the tube. The

6   layers were aspirated, leaving about 500 μL as some cells, depending on their size, usually float in

7   percoll just above the pellet. The cells were then washed once in DPBS making sure not to resuspend

8   the pellet. This was achieved by gently adding 4 ml DPBS, closing the tube and holding it in a

9   horizontal position, and gently tilting it 145 degrees in order to mix the remaining percoll with the

10   added DPBS. The cells were then pelleted by centrifuging them at 400xg for10 minutes at 4°C.

11   In Figure S7 we show the utility and effectiveness of the chosen brain dissociation and cell

12   isolation protocol in obtaining a large amount of microglia and astrocytes from as little as 1 single

13   hippocampus from 1 brain hemisphere of adult male mice. Indeed, enough RNA can be obtained

14   from either microglia or astrocytes from 1 hippocampus to perform scSeq, or to generate an RNA

15   library for bulk sequencing (Figure S7).

16   We further compared the two protocols for their efficiency in producing microglial single cell

17   suspensions and their proportion of live cells via flow cytometry (Figure S6b, c). We found that MD

18   yielded a higher proportion of microglia live cells (Figure S6b) and a higher proportion of microglia

19   singlets (Figure S6c) as compared to ED. We further compared the total amount of single cells that

20   can be obtained from adult mouse glioma samples via our MD as compared to ED. Our MD protocol

21   yielded a higher proportion of singlets (total cells) from tumor-bearing brain hemispheres (Figure

22   S6d). When comparing the percentage of microglial singlets and live cells from tumor bearing

23   hemispheres, we found that the two techniques gave comparable results (Figure S6e). Finally, as

24   displayed in Figure 1B, when using the same number of input cells, a higher proportion of adult

25   mouse hippocampal neurons can be obtained via this method, while a huge proportion of the latter

26   die when using enzymatic digestion.

27

28   **Microglia and Astrocyte Isolation**

1   A schematic illustration of the procedures used for microglia and astrocyte isolation is provided in

2   Figure 3a. For the proteomic analysis, microglia or astrocytes were isolated from 4 hippocampi (2

3   mice/sample) via magnetic-activated cell sorting (MACS) using mouse anti-CD11b (for microglia)

4   or anti-ACSA-2 (for astrocytes) magnetic microbeads (Miltenyi, see Table 1) according to the

5   manufacturer's instructions with some modifications. The MACS buffer used consisted of 1.5%

6   bovine serum albumin (BSA) diluted in DPBS from a commercial 7.5% cell-culture grade BSA stock

7   (Thermo Fisher Scientific). For the isolation of astrocytes, total hippocampal cell pellets after percoll

8   (see above) were re-suspended in 80 μL MACS buffer and 10 μL FcR-blocking reagent (Miltenyi).

9   The cells were then incubated for 10 min at 4°C. Thereafter, 10 μL of anti-ACSA-2 microbeads were

10   added and the cells were incubated for 15 min at 4°C. The cells were then washed with 1 ml MACS

11   buffer and pelleted at 300xg for 5 min at 4°C. The cells were then passed through an MS MACS

12   column attached to a magnet. This led ACSA-2-labeled cells to stay attached to the column, whereas

13   unlabeled cells flowed through the column. After washing the columns three times with MACS

14   buffer, astrocytes were flushed from the column with 1 ml MACS buffer and pelleted at 300xg for 5

15   min at 4°C. Cell pellets were then snap-frozen in liquid nitrogen and stored at -80°C. The same

16   procedures (including the FcR-blocking step) were used to isolate microglia via anti-mouse CD11b

17   microbeads. Figure S7b, d show a qRT-PCR-based ascertainment of microglial or astrocytic cell

18   enrichment after MACS from total brain cells obtained with the 4°C protocol described above (See

19   Additional File 1 for the detailed cell isolation protocol). Cells were counted manually using a

20   standard hemocytometer (NanoEnTek, product code DHC-N01).

21   **RNA Extraction and Quantification**

22   The RNA was extracted via the Lexogen Split-RNA extraction kit (Lexogen) according to the

23   manufacturer's instructions. The kit is based on phenol-chloroform extraction in acidic conditions,

24   and we found this technique to yield the highest amount of RNA. RNA concentrations were measured

25   via Qubit 4 fluorometer (Invitrogen), using the RNA HS Assay kit (Invitrogen).

26

27   **Quantitative Real-Time PCR**

1 RNA was analyzed by TaqMan qRT-PCR instrument (CFX384 real-time system, Bio-Rad

2 Laboratories) using the iTaq™ Universal Probes One-Step Kit for probes (Bio-Rad Laboratories).

3 The samples were run in 384-well formats in triplicates as multiplexed reactions with a normalizing

4 internal control. We chose 36B4 as internal standard for gene expression analyses. Thermal cycling

5 was initiated with an incubation at 50°C for 10 min (RNA retrotranscription) and then at 95°C for 5

6 min (TaqMan polymerase activation). After this initial step, 39 cycles of PCR were performed. Each

7 PCR cycle consisted of heating the samples at 95°C for 10 s to enable the melting process and then

8 for 30 s at 60°C for the annealing and extension reaction. Cutsom-made primers with probes for

9 TaqMan were purchased from Thermo Fisher: housekeeping gene: 36B4, product code:

10 NM_007475.5, Siglech, prduct code: Mm_00618627_m1, P2ry12, product code: Mm00446026_m1,

11 Gfap, product code: Mm01253033_m1, Slc1a3, product code: Mm00600697_m1. Relative target

12 gene expression was calculated according to the Delta C(T) method.

13

14 **Single-cell RNA sequencing (scRNA-seq) using 10X Genomics platform**

15 The quality and concentration of the single cell preparations were evaluated using an

16 haemocytometer in a Leica DM IL LED microscope and adjusted to 1,000 cells/µl. 10,000 cells per

17 sample were loaded into the 10X Chromium controller and library preparation was performed

18 according to the manufacturer's indications (single cell 3' v3 protocol). The resulting libraries were

19 sequenced in an Illumina NovaSeq sequencer according to 10X Genomics recommendations (paired-

20 end reads, R1=28, i7=8, R2=91) to a depth of around 50,000 reads per cell. The quality check

21 outcomes are displayed in Figure S2.

22 **Single-cell RNA-Seq Analysis**

23 10x Chromium data was demultiplexed with cellranger mkfastq v2.0.2.Gene-cell count matrix was

24 generated by cellranger count v2.0.2 against Ensembl GRCm38.p5 reference genome.

25 Single Cell RNA-Seq data analysis was carried out with R Seurat (V3) package. Specifically, to

26 account for potential batch effects, we used canonical correlation analysis (utilized in IntegrateData

27 function) that identifies a linear combination of features to construct a shared correlation structure

28 and align the global transcriptome across 2 datasets (Butler, Hoffman, Smibert, Papalexi, & Satija,

1 2018; Stuart et al., 2019). Only genes that were detected in at least 5 cells were included in the

2 analysis. . Furthermore, we excluded from the analysis all cells with less than 200 or more then 5000

3 genes detected and cells that have more than 25% mitochondrial fraction. We carried out standard

4 preprocessing (log-normalization), and identified the top 2000 variable features for each dataset (37C

5 and 4C). We then identified integration anchors using the FindIntegrationAnchors function. Here

6 we used all default parameters for identifying anchors between the two data sets, setting the

7 'dimensionality' to 1:15. The final batch-corrected expression matrix was created from this anchor-

8 set using IntegrateData function where the number of PCs used for weighting was set to 15. We

9 employed a standard Seurat workflow for clustering and visualization: data scaling, PCA analysis

10 and UMAP clustering using PCA reduction. For improved visualization, we further filtered out all

11 cells located more than 3 standard deviations away from their cluster center and those which had a

12 different identity than the majority of their 10 nearest neighbors in the UMAP.

13 The differential expression analysis was carried out using FindMarker function (logfc.threshold=0).

14 P-values were calculated using Wilcoxon Rank Sum test, and adjusted with Bonferroni correction

15 **Code Availability**

16 A detailed list of commands used to analyze the single cell sequencing data as well as gene count

17 matrixes are available at https://github.com/bihealth/SC-RNA-Seq-37vs4.

18

19 **Proteotype Analysis**

20 □ *Liquid chromatography–tandem mass spectrometry (LC-MS/MS) analysis*

21 The samples used for proteotype analysis were prepared using S-trap (Protifi) columns according to

22 the manufacturer's instructions. For MS analysis, peptides were reconstituted in 5% acetonitrile and

23 0.1% formic acid containing iRT peptides (Biognosys) as described in Escher et al., 2012 (Escher et

24 al., 2012).

25 The peptides resulting from the isolation of microglia were analyzed in data independent

26 acquisition (DIA) and data dependent acquisition (DDA) mode for spectral library generation. For

27 spectral library generation, a fraction of the samples originating from the same condition were pooled

28 to generate mixed pools for each condition. Peptides were separated by reverse-phase

11

1   chromatography on a high-pressure liquid chromatography (HPLC) column (75-μm inner diameter;

2   New Objective) packed in-house with a 50-cm stationary phase ReproSil-Pur 120A C18 1.9 μm (Dr.

3   Maisch GmbH) and connected to an EASY-nLC 1000 instrument equipped with an autosampler

4   (Thermo Fisher Scientific). The HPLC was coupled to a Fusion mass spectrometer equipped with a

5   nanoelectrospray ion source (Thermo Fisher Scientific). Peptides were loaded onto the column with

6   100% buffer A (99% H2O, 0.1% formic acid) and eluted with increasing buffer B (99.9%

7   acetonitrile, 0.1% formic acid) over a nonlinear gradient for 120min. The DIA method (Bruderer et

8   al. 2017) (Bruderer et al., 2017) contained 26 DIA segments of 30,000 resolution with IT set to 60ms,

9   AGC of $3x10_6$, and a survey scan of 120,000 resolution with 60 ms max IT and AGC of $3x10_6$. The

10   mass range was set to 350-1650 m/z. The default charge state was set to 2. Loop count 1 and

11   normalized collision energy was stepped at 27. For the DDA, a 3s cycle time method was recorded

12   with 120,000 resolution of the MS1 scan and 20 ms max IT and AGC of $1x10_6$. The MS2 scan was

13   recorded with 15,000 resolution of the MS1 scan and 120 ms max IT and AGC of $5x10_4$. The covered

14   mass range was identical to the DIA.

15   The peptides resulting from the isolation of astrocytes were analyzed in DIA and DDA mode

16   for spectral library generation. For spectral library generation, a fraction of the samples originating

17   from the same condition were pooled to generate mixed pools for each condition. Peptides were

18   separated by reverse-phase chromatography on a 50cm EASY-Spray C18 LC column (Thermo

19   Fisher Scientific) connected to an EASY-nLC 1200 instrument equipped with an autosampler

20   (Thermo Fisher Scientific). The HPLC was coupled to a Fusion Lumos mass spectrometer equipped

21   with a nanoelectrospray ion source (Thermo Fisher Scientific). Peptides were loaded onto the column

22   with 100% buffer A (99% H2O, 0.1% formic acid) and eluted with increasing buffer B (80%

23   acetonitrile, 0.1% formic acid) over a nonlinear gradient for 120min. The DIA method (Muntel et

24   al., 2019) contained 40 DIA segments of 30,000 resolution with IT set to 55ms, AGC of $1x10_6$, and

25   a survey scan of 120,000 resolution with 50 ms max IT and AGC of $5x10_5$. The mass range was set

26   to 350-1650 m/z. The default charge state was set to 2. Loop count 1 and normalized collision energy

27   was set to 27. For the DDA, a 3s cycle time method was recorded with 120,000 resolution of the

28   MS1 scan and 25 ms max IT and AGC of $5x10_5$. The MS2 scan was recorded with 15,000 resolution

1   of the MS1 scan and 35 ms max IT and AGC of 2×10^4. The covered mass range was identical to the

2   DIA.

3

4   □ *Data analysis DIA LC-MS/MS*

5   LC-MS/MS DIA runs were analyzed with Spectronaut Pulsar X version 12 (Biognosys) (Bruderer et

6   al., 2017) using default settings. Briefly, a spectral library was generated from pooled samples

7   measured in DDA (details above). The collected DDA spectra were searched against UniprotKB

8   (UniProt Swiss-prot, Mus musculus retrieved 2018) using the Sequest HT search engine within

9   Thermo Proteome Discoverer version 2.1 (Thermo Fisher Scientific). We allowed up to two missed

10   cleavages and semi-specific tryptic digestion. Carbamidomethylation was set as a fixed modification

11   for cysteine, oxidation of methionine and deamidation of arginine were set as variable modifications.

12   Monoisotopic peptide tolerance was set to 10 ppm, and fragment mass tolerance was set to 0.02 Da.

13   The identified proteins were assessed using Percolator and filtered using the high peptide confidence

14   setting in Protein Discoverer. Analysis results were then imported to Spectronaut Pulsar version 12

15   (Biognosys) for the generation of spectral libraries.

16   Targeted data extraction of DIA-MS acquisitions was performed with Spectronaut version

17   12 (Biognosys AG) with default settings using the generated spectral libraries as previously described

18   (Bruderer et al., 2017). The proteotypicity filter "only protein group specific" was applied. Extracted

19   features were exported from Spectronaut for statistical analysis with MSstats (version 3.8.6) using

20   default settings (Choi et al., 2014). Briefly, features were filtered for calculation of Protein Group

21   Quantity as defined in Spectronaut settings, common contaminants were excluded. For each protein,

22   features were log-transformed and fitted to a mixed effect linear regression model for each sample

23   in MSstats (Choi et al., 2014). In MSstats, the model estimated fold change and statistical

24   significance for all compared conditions. Significantly different proteins were determined by the

25   threshold fold-change > 2 and adjusted p-value < 0.01. Benjamini-Hochberg method was used to

26   account for multiple testing.

27

28   **Data Accessibility**

13

1   The raw data for the single-cell sequencing will be made publicly available before publication with

2   associated access code and web link. All mass spectrometric data and acquisition information were

3   deposited to the ProteomeXchange Consortium (www.proteomexchange.org/) via the PRIDE partner

4   repository (Perez-Riverol et al., 2019) (data set identifier: PXD015592,

5   username: reviewer08386@ebi.ac.uk, password: kRa2alY7).

6

7   **Gene Ontology Analysis**

8   The functional enrichment analysis for the transcriptome data was carried out with R tmod package

9   (Zyla et al., 2019), using Utest. For each cell type we used genes that were detected by

10 Seurat::FindMarker (logfc.threshold=0) function and sorted them by adjusted P-values: microglia –

11 5631 genes, astrocytes – 4108 genes, and neurons – 3288 genes. The enrichment analysis is done

12 using GO gene set collection from MsigDB. To match MsigDB gene symbols, mouse gene ids were

13 converted to upper case. Significantly enriched gene sets remain significant if hypergeometric test is

14 used, for example via GOrilla, (data not shown). Significantly different genes were determined by

15 the threshold: log-fold change > 0.5, adjusted p-value cut-off < 0.01. Table S1 contains a full list of

16 deregulated genes for all cells and Table S2 contains the full GO-analysis of deregulated genes for

17 each cell type analysed. For the proteomic GO analysis, we used hypergeometric test from the

18 GOrilla online tool (Eden, Navon, Steinfeld, Lipson, & Yakhini, 2009). For the proteomic GO

19 analysis, we used the hypergeometric test from GOrilla online tool: all quantified microglial or

20 astrocytic proteins were used as background, while the significantly deregulated proteins were used

21 as target set (all as Uniprot IDs, log-fold change > 2, adjusted p-value cut-off < 0.01). Significantly

22 up- and downregulated proteins were analyzed separately using the same background set of proteins.

23 Table S3 and Table S4 contains the full list of deregulated proteins and GO analysis per cell type

24 respectively.

25 **Comparison of RNA and Protein Expression Changes**

26 In astrocytes, we quantified 3823 proteins present in both conditions (ED and MD), which were

27 assigned to 3623 unique genes. Median log-fold changes (LFCs) were used for the comparison of

28 RNA and protein expression changes. For microglia, we quantified 4328 proteins that were present

1   in both conditions (ED and MD), and these were assigned to 4158 unique genes. Pearson's

2   correlation was used to assess the linear association between the datasets.

3   **Table 2:** List of antibodies used for the flow cytometric analysis.

Antigen	Clone	Color	Vendor	Product #
CD11b clone M1/70	M1/70	BV711	Biolegend	101242
CD11b clone M1/70	M1/70	APC-Cy7	Biolegend	101226
CD45 clone 30-F11	30-F11	Pacific Blue	Biolegend	103126
CD45 clone 30-F11	30-F11	PerCP/Cy5.5	Biolegend	103131
FcγRI (CD64), clone X54-5/7.1	X54-5/7.1	BV605	Biolegend	139323
FcγRI (CD64), clone X54-5/7.1	X54-5/7.1	PE-Dazzle594	Biolegend	139319
Cd172a (SIRPα), clone P84	P84	PE-Cy7	Biolegend	144007
Cd172a (SIRPα), Cd172a (SIRPα), clone P84	P84	Alexa Fluor 700	Biolegend	144021
Fixable Viability Kit	N/A	AmCyan	Biolegend	423102

4

5   **Flow Cytometric Analysis**

6   Data analysis was performed using FlowJo 10.0.x (Treestar). Populations of interest were manually

7   pre-gated in FlowJo software. Microglia were identified as $CD45_{medium}$ $CD11b_{medium}$, live, single cells.

8   After preprocessing we combined equal number of randomly selected cells from each group and

9   visualized data using t-Distributed Stochastic Neighbor Embedding (t-SNE). The reagents used in

10 flow cytometry are summarized in Table 2 below.

11   One hippocampus/sample (from 1 brain hemisphere) was used for the fluorescence activated

12 cell sorting (FACS) experiments. Cells were isolated as described above. After cell isolation, the

13 samples were washed with PBS and stained for surface markers and live/dead reagent. Following

14 washing with PBS, the cells were fixed and permeabilized with Cytofix/Cytoperm (BD, #554715),

15 followed by staining for intracellular markers. Flow cytometry was performed on an LSR II Fortessa

16 (equipped with 405 nm, 488 nm, 561 nm and 640 nm laser lines; special order research product, BD)

17 with FACS Diva Software. Before acquisition, PMT voltages were manually adjusted to reduce

18 fluorescence spillover, and single- stain controls were acquired for compensation matrix calculation.

19

20

1 **Results**

2 **Enzymatic tissue digestion induces transcriptional biases in brain cells**

3 First, we compared single cell suspensions obtained by 30-min ED at 37°C or MD at 4°C from

4 mouse hippocampal tissue (Figure 1a; MD-protocol was optimized in-house, see material and

5 methods and Additional File 1 for the detailed protocol). The hippocampus was selected because it

6 represents a discrete brain region that can be dissected in a consistent way. Visual inspection of the

7 isolated cells showed that ED considerably affected cell morphology as compared to MD, with ED-

8 processed cells being consistently smaller in size (Figure 1a).

9 We then conducted single-cell RNA-sequencing (scRNA-seq) to compare the transcriptional

10 profile of hippocampal cell suspensions generated via both techniques. Quality check for the scRNA-

11 seq is provided in Figure S2. Clustering using specific gene-set enrichment for cell-type

12 identification (Hamilton, White, Rees, Wheeler, & Ascoli, 2017; Saunders et al., 2018) (Figure 1b)

13 revealed quantitative and qualitative differences in cellular subpopulations between ED and MD. It

14 appears evident that in tissue processed at 37°C there is a higher extent of cell death among sensitive

15 populations, e.g. neurons and astrocytes, shifting the balance towards a higher proportion of

16 microglia cells. Indeed, the cell population ratios seen in the MD condition are closer the known

17 biological cellular proportions (Keller, Ero, & Markram, 2018). The differential gene expression

18 analysis showed that ED causes significant transcriptional changes in microglia (226 deregulated

19 genes), astrocytes (290 deregulated genes) and neurons (771 deregulated genes), (Figure 2a). We

20 also found transcriptional deregulation in other main brain cell types, including oligodendrocytes

21 (369 genes), endothelial cells (128 genes), border associated macrophages (134 genes), neuronal

22 precursor cells (121 genes), fibroblast-like cells (480 genes) and mural cells (223 genes) (Figure S3a,

23 b; a complete list of differentially expressed genes is provided in Table S1). Gene ontology (GO)

24 analysis revealed that ED induced global deregulation in genes associated with e.g. RNA-editing,

25 translation, metabolic functions in most cells and also immune pathways deregulation in microglia

26 cells (Figure 2c, Figure S3; Table S2 contains the complete GO-analysis). In addition, ED led to the

27 emergence of a distinct microglial subpopulation that was barely represented in cell suspensions

28 obtained via MD (Figure 2b). The latter subpopulation was characterized by increased expression of

16

1   immediate early genes such as *Jun, Fos* (Figure 2b), and also Egr1, Hspa8 and Jund (Figure S4)

2   reflecting an immediate microglial response to the ED. Increased immediate early gene expression

3   along with deregulation in genes encoding for ribosomal and mitochondrial proteins (Rpl, Rps and

4   mt-genes) was a common feature for most brain cells exposed to ED conditions (Table S1, Figure

5   S4). Deregulation in the latter genes has also been observed in peripheral tissues following ED (van

6   den Brink et al., 2017), confirming what we report here. These data revealed that, alongside genes

7   that are commonly deregulated upon enzymatic digestion, there are others which are specific to

8   individual cell subtypes, which can be accounted for only by a tissue and cell specific analysis like

9   the present one (Table S1 and S2, Figure S4).

10

11   **Enzymatic tissue digestion causes widespread proteotype artefacts in microglia and astrocytes**

12   Despite the increasing number of studies performing proteotype analysis of brain cells freshly

13   isolated via ED (Flowers, Bell-Temin, Jalloh, Stevens, & Bickford, 2017; Haage et al., 2019; Sharma

14   et al., 2015), it remains unexplored whether ED introduces biological artefacts in proteotype profiles

15   of brain cells. Therefore, we investigated whether the type of cell isolation method could also alter

16   the proteotype of brain cells. To this end, we focused on astrocytes and microglia (Figure 3a), as they

17   are most commonly acutely isolated for proteotype studies (Wilson & Nairn, 2018). Notably,

18   proteotype analysis of freshly isolated brain cells is a current challenge in the field (Wilson & Nairn,

19   2018). We here demonstrate that our MD protocol followed by the S-trap method for protein

20   extraction and peptide preparation enables solid mass spectrometry analyses of microglia and

21   astrocytes extracted from only four adult mouse hippocampi (see Material and Methods).

22   Consistent with the effects on the transcriptome (Figure 2), proteotype analysis using data-

23   independent acquisition (DIA)-based liquid chromatography–tandem mass spectrometry (LC-

24   MS/MS) revealed marked differences between the proteotype of microglia (Figure 3b) and astrocytes

25   (Figure 3c) isolated via ED or MD. In microglia, 1619 proteins were significantly different after ED

26   compared to MD. For astrocytes, we found 1984 to be significantly different following ED compared

27   to MD. GO analysis of deregulated microglial proteins revealed that ED altered the level of proteins

28   involved in cell motility, endocytosis, and immune processes, as well as proteins pertaining to mRNA

1   editing, histone modifications and chromatin architecture (Figure 3b). In astrocytes, ED induced

2   alterations in proteins associated with various metabolic processes, and with modifications in the

3   translational and transcriptional machinery, similar to the effects on the microglial proteotype (Figure

4   3c).

5   We identified a remarkable consistency and correspondence between the effects of ED on

6   transcriptomic and proteotype changes in both glial cell types. In fact, the top 50 deregulated RNAs

7   significantly correlated with changes of the corresponding proteins in microglia (Figure 3d, R = 0.49,

8    $p = 0.00027$) and astrocytes (Figure 3e, R = 0.29, $p = 0.043$). Thus, our findings show that ED is able

9   to induce cell responses that lead to a substantial alteration in glia cell proteotype. A complete list of

10   deregulated proteins and GO analysis is provided in Table S3 and Table S4.

11   Of note, in case of animal perfusion with buffers at room temperature (RT) rather than at 4°C, a

12   thermal shift from RT to 37°C could still represent a biological shock (Mahat et al., 2016). We

13   therefore screened whether perfusion at RT and subsequent ED at 37°C induced the same degree of

14   proteotype alterations in microglia cells as compared to perfusion with cold buffers and subsequent

15   ED or MD (Figure S5). We found that changes in proteotype were independent of the range of

16   thermal shock between perfusion temperature and subsequent dissociation step at 37°C (Figure S5).

17

18   **Enzymatic tissue digestion alters the detection of classical microglial markers by flow**

19   **cytometry**

20   Finally, we also examined the influence of different cell isolation techniques on fluorescence-

21   activated cell sorting (FACS). While ED is frequently used to produce single cell suspensions for

22   subsequent FACS analysis of microglia (Chen et al., 2012; Martin, Boucher, Fontaine, & Delarasse,

23   2017; Mrdjen et al., 2018), to our knowledge no study has yet examined how cell responses during

24   ED might influence subsequent flow cytometry analysis. Therefore, we compared whether ED,

25   relative to MD, alters the expression of classical immune markers used in FACS-based analyses of

26   microglia. FACS analysis confirmed that our MD protocol yielded cells of larger size than ED, as

27   demonstrated by a significantly higher forward scatter (Figure 4a-c; gating strategy in Figure S6a).

28   We then compared the relative expression levels of the commonly used microglial markers CD45,

1   CD11b, SIRP-α and FcγR1 between the two methods, both on the surface and intracellularly, using

2   differentially labelled antibodies. Surface expression was significantly increased for CD11b, CD45

3   and SIRP-α in ED-isolated cells compared to cells obtained via MD (Figure 4d-g). The increase in

4   the intracellular staining of CD11b indicates a significant internalization after ED (Figure 4h, i),

5   consistent with the increase in endocytosis-related proteins observed in the proteotype analysis.

6   Moreover, intracellular CD11b expression was the main discriminating factor when the MD and ED

7   conditions were clustered together (Figure 4h). Thus, the cell isolation method can influence the

8   cellular indices used to select and study microglial cell populations in FACS-analysis. Of note, the

9   present FACS analysis demonstrated that our MD protocol yielded a higher percentage of microglial

10   singlets and live cells as compared ED (Figure S6b, c), showing that enzymes are not strictly

11   necessary to obtain a successful single cell suspension.

12

Discussion

14   We here provide a systematic investigation of the influence of different cell isolation protocols on

15   transcriptional and proteotype profiles in mouse brain tissue, by taking into account single-cell

16   transcriptomics of brain cells, proteotypes of microglia and astrocytes, and FACS analysis of

17   microglia. Our findings indicate that ED-based cell isolation induces alterations in gene and protein

18   expression involving both up- and downregulations. We hypothesize that such changes are due to a

19   cellular response to the thermal shock suffered by the cells and to their response to the

20   microenvironment present during enzymatic digestion. These alterations are likely to introduce

21   undesirable biological biases in brain cell specific transcriptomic and proteotype profiling. While the

22   potential risk of introducing biological artefacts through the use of ED-based cell isolation techniques

23   has received recent attention in the context of transcriptomic studies (Ayata et al., 2018; Hrvatin et

24   al., 2018; Wu et al., 2017), our work is the first to systematically and specifically address this issue

25   and to extend this concern to proteotype and flow cytometry analyses. The latter is of particular

26   importance given the increasing use of ED in mass-cytometry to study and characterize brain immune

27   cells (Ajami et al., 2018; Bottcher et al., 2019; Mrdjen et al., 2018).

1   Efforts towards minimizing bias in transcriptomic datasets are indispensable not only for

2   enhancing the reproducibility of findings, but also to avoid biological misinterpretation of datasets

3   within studies. A way to obviate such biases is the use of single nucleus sequencing (snSeq), where

4   whole tissue is homogenized and cells are lysed to release single nuclei that can be processed for

5   sequencing (Bakken et al., 2018; Liu et al., 2019). This method is at present prevalently used for

6   frozen human brain tissue samples (Habib et al., 2017), and represents a good alternative for single

7   cell characterization of brain cells with less depth as compared to ordinary scSeq (Bakken et al.,

8   2018). Nevertheless, snSeq is not applicable for studies requiring brain cell-specific bulk sequencing

9   of e.g. freshly isolated microglia, to achieve a higher sequencing depth. In a few instances, scientists

10   have adopted the use of transcription and translation blockers to avoid transcriptional and

11   translational responses that can occur during ED (Hrvatin et al., 2018; Wu et al., 2017). However,

12   while this strategy might be efficient in preventing *de novo* gene and protein expression, it does not

13   prevent degradation/downregulation of pre-existing RNAs and proteins, which according to the

14   present data, occurs during ED-based isolation as compared to MD at 4°C. Moreover, our proteotype

15   analysis of microglia and astrocytes revealed that ED induced the deregulation of proteins associated

16   with various epigenetic processes, including chromatin remodelling, histone modifications and DNA

17   methylation (Figure 3, Tables S3 and S4). ED thus likely modifies the epigenetic machinery, which

18   cannot be prevented via transcription and/or translation blockers. The latter will also not avert

19   changes in FACS analyses of brain cells such as microglia. Indeed, here we show that ED leads to

20   an increase in proteins associated with endocytosis (see GO table in Figure 3b) and to a marked

21   internalization of a microglial cell marker (CD11b) as compared to MD as well as to alterations in

22   relative expression of surface markers (Figure 4). It has to be stressed that both mechanical

23   dissociation and ED, will alter the surface of cells due to mechanical stress and enzymatic trimming

24   respectively, which *per se* introduces a degree of technical bias in both cases. However, holding cells

25   in a metabolically quiescent state will prevent processes such as endocytosis and degradation that

26   might further alter the intracellular/surface protein levels. In general, it can be argued that ED is often

27   chosen because of difficulty in tissue dissociation, as is the case with e.g. brain tumors. We here

28   provide evidence that the proposed mechanical dissociation protocol is efficient also with adult

1   mouse brain tumors (Figure S6d). Human brain tumors might be more challenging and require

2   enzymatic digestion. For these cases we would suggest enzyme mixes which work at cold

3   temperatures such as Accutase, that can be complemented with a finishing round of Dounce

4   homogenization as performed for the ED protocol used in the present study (see methods and

5   Additional File 1).

6   Our findings corroborate the data generated by van den Brink et al. (van den Brink et al., 2017),

7   who identified transcriptomic bias in peripheral tissue cells isolated via ED (e.g. pancreatic cells and

8   muscle stem cells). This consistency is particularly remarkable when considering the ED-mediated

9   deregulation in genes associated with translation, RNA processing and cellular metabolism. The

10 latter study has been used by the authors of the *Tabula Muris* as a reference database to remove ED-

11 induced genes bioinformatically *a posteriori* from the single cell transcriptional atlas produced in

12 various mouse organs (Tabula Muris et al., 2018). However, the work by van den Brink et al. only

13 considered genes that were upregulated upon ED, while not accounting for potential downregulation

14 of genes. Our study shows that the latter can occur as well. For instance, of the 771 significantly

15 deregulated genes in neurons, 586 were downregulated, while of the 226 significantly deregulated

16 microglial genes, 118 were downregulated (Table S1). Likewise, according to our proteotype

17 analysis, ED caused the downregulation of 772 proteins in microglia and of 1230 proteins in

18 astrocytes (Table S3). Moreover, beside the general consistency between our findings and those

19 reported by van den Brink et al., we identified several brain cell-specific alterations in biological

20 processes after ED, which could not have been predicted by analyses of peripheral cells. A recent

21 study by Ayata et al. also raised this issue by comparing microglia isolated via enzymatic digestion

22 with microglial specific mRNA isolated via the translating ribosome affinity purification (TRAP)

23 method (Ayata et al., 2018). They noted an increased expression of immediate early genes and

24 immune related genes in their bulk sequencing of frehsly isolated microglia cells, in line with what

25 we observe in this study. This indicates that ED-induced artifacts appear not only in scSeq, but also

26 in bulk sequencing. In the present study, we describe an optimized protocol which provide an

27 effective alternative to the use of transgenic mice lines involving TRAP technology or expensive

28 dossiciation machines and enzymes (Additional File 1). The MD procedure at cold temperature here

1   described yields a more representative picture of the cell populations due to less cell death and higher

2   cell recovery.

3

4   In summary, although any brain cell isolation method available at present will bear a degree of

5   technical and biological artefacts, cold MD of brain tissue helps minimize the profound alterations

6   in the transcriptome and proteotype of specific brain cells, as seen after standard ED at 37°C. Our

7   dataset provides a mean of identifying brain-cell specific genes and proteins affected by ED, that can

8   be useful for correction when using previously published data sets produced via ED. Finally, we

9   disclose a cost-effective, easily established and optimized MD protocol at 4°C which will be useful

10   for the neuroscientific community.

11

22   **Competing interests**

23   Unrelated to the present study, U.M. has received financial support from Boehringer Ingelheim

24   Pharma GmbH & Co. and from and Wren Therapeutics Ltd. All other authors have no competing

25   interests.

26   **Author contributions**

27   D.M., A.I., R.C.P., B.W., D.B., J.v.B. and U.M. conceived and designed the study. D.M., A.I.,

28   M.v.O., S.P, J.R., F.M., M.R., M.M.B., L.S., performed the experiments and analysed the data. D.M.,

R.C.P., and U.M. wrote the manuscript. All authors discussed the results and commented on the manuscript.

References

Ajami, B., Samusik, N., Wieghofer, P., Ho, P. P., Crotti, A., Bjornson, Z., . . . Steinman, L. (2018). Single-cell mass cytometry reveals distinct populations of brain myeloid cells in mouse neuroinflammation and neurodegeneration models. *Nat Neurosci, 21*(4), 541-551. doi:10.1038/s41593-018-0100-x

Ayata, P., Badimon, A., Strasburger, H. J., Duff, M. K., Montgomery, S. E., Loh, Y. E., . . . Schaefer, A. (2018). Epigenetic regulation of brain region-specific microglia clearance activity. *Nat Neurosci, 21*(8), 1049-1060. doi:10.1038/s41593-018-0192-3

Bakken, T. E., Hodge, R. D., Miller, J. A., Yao, Z., Nguyen, T. N., Aevermann, B., . . . Tasic, B. (2018). Single-nucleus and single-cell transcriptomes compared in matched cortical cell types. *PLoS One, 13*(12), e0209648. doi:10.1371/journal.pone.0209648

Beffinger, M., Schellhammer, L., Pantelyushin, S., & Vom Berg, J. (2019). Delivery of Antibodies into the Murine Brain via Convection-enhanced Delivery. *J Vis Exp*(149). doi:10.3791/59675

Bottcher, C., Schlickeiser, S., Sneeboer, M. A. M., Kunkel, D., Knop, A., Paza, E., . . . Priller, J. (2019). Human microglia regional heterogeneity and phenotypes determined by multiplexed single-cell mass cytometry. *Nat Neurosci, 22*(1), 78-90. doi:10.1038/s41593-018-0290-2

Bruderer, R., Bernhardt, O. M., Gandhi, T., Xuan, Y., Sondermann, J., Schmidt, M., . . . Reiter, L. (2017). Optimization of Experimental Parameters in Data-Independent Mass Spectrometry Significantly Increases Depth and Reproducibility of Results. *Mol Cell Proteomics, 16*(12), 2296-2309. doi:10.1074/mcp.RA117.000314

Butler, A., Hoffman, P., Smibert, P., Papalexi, E., & Satija, R. (2018). Integrating single-cell transcriptomic data across different conditions, technologies, and species. *Nat Biotechnol, 36*(5), 411-420. doi:10.1038/nbt.4096

Chen, Z., Jalabi, W., Shpargel, K. B., Farabaugh, K. T., Dutta, R., Yin, X., . . . Trapp, B. D. (2012). Lipopolysaccharide-induced microglial activation and neuroprotection against experimental brain injury is independent of hematogenous TLR4. *J Neurosci, 32*(34), 11706-11715. doi:10.1523/JNEUROSCI.0730-12.2012

1 Choi, M., Chang, C. Y., Clough, T., Broudy, D., Killeen, T., MacLean, B., & Vitek, O. (2014).
2   MSstats: an R package for statistical analysis of quantitative mass spectrometry-based
3   proteomic   experiments.   *Bioinformatics,   30*(17),   2524-2526.
4   doi:10.1093/bioinformatics/btu305

5 Eden, E., Navon, R., Steinfeld, I., Lipson, D., & Yakhini, Z. (2009). GOrilla: a tool for discovery
6   and visualization of enriched GO terms in ranked gene lists. *BMC Bioinformatics, 10*, 48.
7   doi:10.1186/1471-2105-10-48

8 Escher, C., Reiter, L., MacLean, B., Ossola, R., Herzog, F., Chilton, J., . . . Rinner, O. (2012). Using
9   iRT, a normalized retention time for more targeted measurement of peptides. *Proteomics,
10   12*(8), 1111-1121. doi:10.1002/pmic.201100463

11 Flowers, A., Bell-Temin, H., Jalloh, A., Stevens, S. M., Jr., & Bickford, P. C. (2017). Proteomic
12   anaysis of aged microglia: shifts in transcription, bioenergetics, and nutrient response. *J
13   Neuroinflammation, 14*(1), 96. doi:10.1186/s12974-017-0840-7

14 Fujita, J. (1999). Cold shock response in mammalian cells. *J Mol Microbiol Biotechnol, 1*(2), 243-
15   255. Retrieved from https://www.ncbi.nlm.nih.gov/pubmed/10943555

16 Haage, V., Semtner, M., Vidal, R. O., Hernandez, D. P., Pong, W. W., Chen, Z., . . . Gutmann, D. H.
17   (2019). Comprehensive gene expression meta-analysis identifies signature genes that
18   distinguish microglia from peripheral monocytes/macrophages in health and glioma. *Acta
19   Neuropathol Commun, 7*(1), 20. doi:10.1186/s40478-019-0665-y

20 Habib, N., Avraham-Davidi, I., Basu, A., Burks, T., Shekhar, K., Hofree, M., . . . Regev, A. (2017).
21   Massively parallel single-nucleus RNA-seq with DroNc-seq. *Nat Methods, 14*(10), 955-958.
22   doi:10.1038/nmeth.4407

23 Hamilton, D. J., White, C. M., Rees, C. L., Wheeler, D. W., & Ascoli, G. A. (2017). Molecular
24   fingerprinting of principal neurons in the rodent hippocampus: A neuroinformatics approach.
25   *J Pharm Biomed Anal, 144*, 269-278. doi:10.1016/j.jpba.2017.03.062

26 Hrvatin, S., Hochbaum, D. R., Nagy, M. A., Cicconet, M., Robertson, K., Cheadle, L., . . . Greenberg,
27   M. E. (2018). Single-cell analysis of experience-dependent transcriptomic states in the
28   mouse visual cortex. *Nat Neurosci, 21*(1), 120-129. doi:10.1038/s41593-017-0029-5

29 Keller, D., Ero, C., & Markram, H. (2018). Cell Densities in the Mouse Brain: A Systematic Review.
30   *Front Neuroanat, 12*, 83. doi:10.3389/fnana.2018.00083

1   Liu, F., Zhang, Y., Zhang, L., Li, Z., Fang, Q., Gao, R., & Zhang, Z. (2019). Systematic comparative
2   analysis of single-nucleotide variant detection methods from single-cell RNA sequencing
3   data. *Genome Biol, 20*(1), 242. doi:10.1186/s13059-019-1863-4

4   Mahat, D. B., Salamanca, H. H., Duarte, F. M., Danko, C. G., & Lis, J. T. (2016). Mammalian Heat
5   Shock Response and Mechanisms Underlying Its Genome-wide Transcriptional Regulation.
6   *Mol Cell, 62*(1), 63-78. doi:10.1016/j.molcel.2016.02.025

7   Martin, E., Boucher, C., Fontaine, B., & Delarasse, C. (2017). Distinct inflammatory phenotypes of
8   microglia and monocyte-derived macrophages in Alzheimer's disease models: effects of
9   aging and amyloid pathology. *Aging Cell, 16*(1), 27-38. doi:10.1111/acel.12522

10 Mattei, D., Ivanov, A., Ferrai, C., Jordan, P., Guneykaya, D., Buonfiglioli, A., . . . Wolf, S. A. (2017).
11   Maternal immune activation results in complex microglial transcriptome signature in the
12   adult offspring that is reversed by minocycline treatment. *Transl Psychiatry, 7*(5), e1120.
13   doi:10.1038/tp.2017.80

14 Mrdjen, D., Pavlovic, A., Hartmann, F. J., Schreiner, B., Utz, S. G., Leung, B. P., . . . Becher, B.
15   (2018). High-Dimensional Single-Cell Mapping of Central Nervous System Immune Cells
16   Reveals Distinct Myeloid Subsets in Health, Aging, and Disease. *Immunity, 48*(3), 599.
17   doi:10.1016/j.immuni.2018.02.014

18 Muntel, J., Kirkpatrick, J., Bruderer, R., Huang, T., Vitek, O., Ori, A., & Reiter, L. (2019).
19   Comparison of Protein Quantification in a Complex Background by DIA and TMT
20   Workflows with Fixed Instrument Time. *J Proteome Res, 18*(3), 1340-1351.
21   doi:10.1021/acs.jproteome.8b00898

22 Perez-Riverol, Y., Csordas, A., Bai, J., Bernal-Llinares, M., Hewapathirana, S., Kundu, D. J., . . .
23   Vizcaino, J. A. (2019). The PRIDE database and related tools and resources in 2019:
24   improving support for quantification data. *Nucleic Acids Res, 47*(D1), D442-D450.
25   doi:10.1093/nar/gky1106

26 Reichard, A., & Asosingh, K. (2019). Best Practices for Preparing a Single Cell Suspension from
27   Solid Tissues for Flow Cytometry. *Cytometry A, 95*(2), 219-226. doi:10.1002/cyto.a.23690

28 Saunders, A., Macosko, E. Z., Wysoker, A., Goldman, M., Krienen, F. M., de Rivera, H., . . .
29   McCarroll, S. A. (2018). Molecular Diversity and Specializations among the Cells of the
30   Adult Mouse Brain. *Cell, 174*(4), 1015-1030 e1016. doi:10.1016/j.cell.2018.07.028

Sharma, K., Schmitt, S., Bergner, C. G., Tyanova, S., Kannaiyan, N., Manrique-Hoyos, N., . . . Simons, M. (2015). Cell type- and brain region-resolved mouse brain proteome. *Nat Neurosci, 18*(12), 1819-1831. doi:10.1038/nn.4160

Stuart, T., Butler, A., Hoffman, P., Hafemeister, C., Papalexi, E., Mauck, W. M., 3rd, . . . Satija, R. (2019). Comprehensive Integration of Single-Cell Data. *Cell, 177*(7), 1888-1902 e1821. doi:10.1016/j.cell.2019.05.031

Tabula Muris, C., Overall, c., Logistical, c., Organ, c., processing, Library, p., . . . Principal, i. (2018). Single-cell transcriptomics of 20 mouse organs creates a Tabula Muris. *Nature, 562*(7727), 367-372. doi:10.1038/s41586-018-0590-4

Tiklova, K., Bjorklund, A. K., Lahti, L., Fiorenzano, A., Nolbrant, S., Gillberg, L., . . . Perlmann, T. (2019). Single-cell RNA sequencing reveals midbrain dopamine neuron diversity emerging during mouse brain development. *Nat Commun, 10*(1), 581. doi:10.1038/s41467-019-08453-1

van den Brink, S. C., Sage, F., Vertesy, A., Spanjaard, B., Peterson-Maduro, J., Baron, C. S., . . . van Oudenaarden, A. (2017). Single-cell sequencing reveals dissociation-induced gene expression in tissue subpopulations. *Nat Methods, 14*(10), 935-936. doi:10.1038/nmeth.4437

Wilson, R. S., & Nairn, A. C. (2018). Cell-Type-Specific Proteomics: A Neuroscience Perspective. *Proteomes, 6*(4). doi:10.3390/proteomes6040051

Wu, Y. E., Pan, L., Zuo, Y., Li, X., & Hong, W. (2017). Detecting Activated Cell Populations Using Single-Cell RNA-Seq. *Neuron, 96*(2), 313-329 e316. doi:10.1016/j.neuron.2017.09.026

Zhang, Y., Chen, K., Sloan, S. A., Bennett, M. L., Scholze, A. R., O'Keeffe, S., . . . Wu, J. Q. (2014). An RNA-sequencing transcriptome and splicing database of glia, neurons, and vascular cells of the cerebral cortex. *J Neurosci, 34*(36), 11929-11947. doi:10.1523/JNEUROSCI.1860-14.2014

Zyla, J., Marczyk, M., Domaszewska, T., Kaufmann, S. H. E., Polanska, J., & Weiner, J. (2019). Gene set enrichment for reproducible science: comparison of CERNO and eight other algorithms. *Bioinformatics, 35*(24), 5146-5154. doi:10.1093/bioinformatics/btz447

1 **Figure Legends**

2

3 **Figure 1. The cell isolation method affects the proportions of murine hippocampal cell**

4 **populations.**

5 **(a)** Schematic illustration of the two cell isolation methods. Adult murine hippocampi were

6 mechanically dissociated at 4°C (MD) or digested enzymatically for 30-min at 37°C (ED). After

7 myelin removal, total hippocampal cells from both conditions were subjected to scRNA-seq. The

8 photomicrographs show the shape of cells isolated via MD or ED. Note that cells isolated via MD

9 appear larger and display discernible nuclei and cytoplasm. **(b)** Uniform manifold approximation and

10 projection (UMAP) scores showing the clustering of cells isolated via ED (4448 cells) or MD (11868

11 cells). **(c)** Coloured legends (left) represent the identities and total fractions for each cell type and the

12 violin plots (right) show the cell identity based on the enriched expression of specific genes.

13

14 **Figure 2. The cell isolation protocol alters the transcriptional profile of mouse hippocampal**

15 **glia and neuronal cells.**

16 **(a)** Scatter plots of the differential gene expression in microglia, astrocytes, and neurons obtained via

17 ED relative to MD. Some examples of up- and downregulated genes following ED are highlighted

18 in red in the scatterplots. **(b)** Feature plot magnification of the microglial population from adult

19 mouse hippocampi displaying the expression of the immediate early genes *Jun* and *Fos*. Enzymatic

20 digestion (ED) at 37°C induces the appearance of a microglial population characterized by increased

21 expression of immediate early genes (upper panel) which is barely present in microglia from

22 hippocampi processed via mechanical dissociation (MD) at 4°C (lower panel). **(c)** Selected gene

23 ontology (GO) terms associated with significantly deregulated genes in microglia, astrocytes and

24 neurons (ED relative to MD). The bar color represents downregulation in ED relative to MD (blue)

25 and upregulation in ED relative to MD (red). The intensity of the respective color indicates the

26 adjusted *p*-value, while the size of the bars denotes the effect size, i.e. the area under the curve (AUC,

27 see Fig. S3b). Significantly different genes were determined by the threshold: log-fold change > 0.5,

28 adjusted *p*-value cut-off < 0.01.

1

2 **Figure 3. The cell isolation method affects the proteotype profiles of mouse microglia and**

3 **astrocytes.**

4 (**a**) Schematic illustration of the main experimental procedure. Adult murine hippocampi were

5 mechanically dissociated at 4°C (MD) or digested enzymatically for 30 min at 37°C (ED). After

6 myelin removal, microglia or astrocytes where freshly isolated via magnetic associated cell sorting

7 (MACS) for cell-specific proteotype analysis. (**b,c**) Volcano plots (top) and select gene ontology

8 (GO) terms (bottom) of deregulated proteins in *(b)* microglia and *(c)* astrocytes obtained via ED

9 relative to MD. N= 4 biological replicates/group. Significantly different proteins were determined by

10 the threshold: fold-change > 2 and adjusted *p*-value < 0.01. Benjamini-Hochberg method was used

11 to account for multiple testing. (**d,e**) Comparison of *(d)* microglial and *(e)* astrocytic RNA and protein

12 expression differences between the two protocols. The top 50 differentially expressed genes (sorted

13 by RNA adj. p-value), which were detected at both RNA and protein levels, are highlighted in the

14 scatterplots. A significant correlation was detected for both microglia (R = 0.49, p = 0.00027) and

15 astrocytes (R = 0.29, p = 0.043).

16

17 **Figure 4. Cell isolation method affects microglial surface and intracellular marker expression**

18 **in flow cytometric analysis.**

19 Flow cytometric analysis of surface and intracellular marker expression levels on microglia after

20 enzymatic digestion (ED) at 37oC versus mechanical dissociation (MD) at 4oC. (**a**) Representative

21 2D-plot overlay with adjunct histograms and (**b**) scatterplots comparing forward scatter (FSC-A, t_8

22 = 5.439, p = 0.0006) and side scatter (SSC-A, t_8 = 18, p < 0.0001). (**c**) Photomicrographs illustrating

23 the cell shape after MD or ED. (**d-g**) Representative 2D-FACS plot overlays with adjunct histograms

24 and scatter plots comparing geometric mean fluorescence intensities (gMFIs) of surface and

25 intracellular expression of *(D)* CD45 (t_8 = 13.28, p < 0.0001), *(E)* CD11b (t_8 = 5.288, p = 0.0007),

26 *(F)* SIRPα (t_8 = 5.213, p = 0.0004) and *(G)* FcγRI, (t_8 = 1.030, p = 0.3). (**h**) A t-SNE clustering

27 algorithm was used to depict CD11b expression in different populations of microglia. Left row

28 showing relative intracellular CD11b expression levels for both conditions. Right row shows overlay

28

1   of the two conditions, as well as all populations overlaid with high CD11b ICS expression. **(i)**

2   Scatterplot for the quantification of the CD11b intracellular signal for microglia isolated via MD

3   versus ED ($t_8 = 24.43$, $p < 0.0001$) Summary of two independent experiments, N= 4 and 5 biological

4   replicates/group respectively. Unpaired two-tailed Student *t*-tests were used to compare the means.
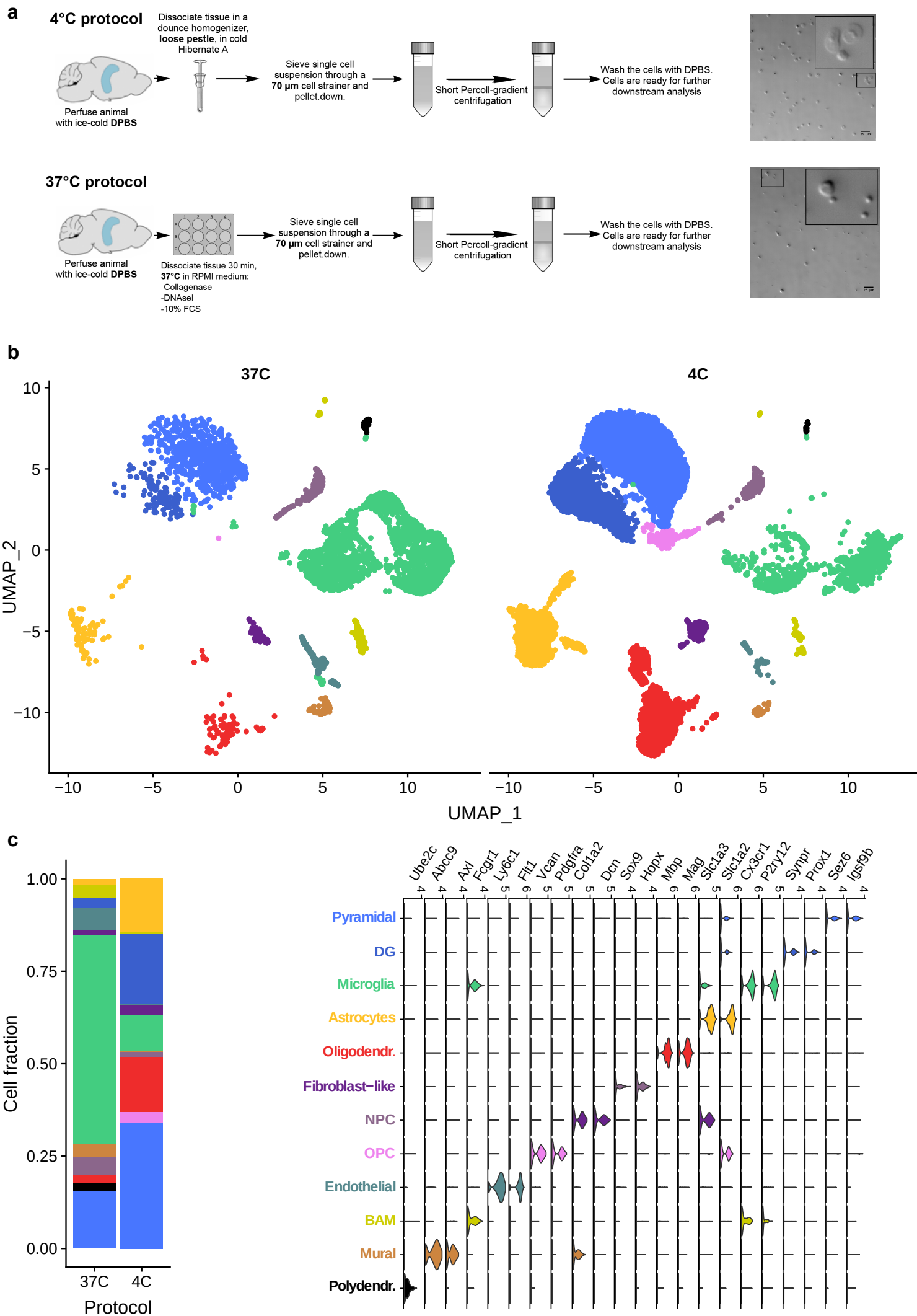
5   Error bars represent the mean ± standard deviation.
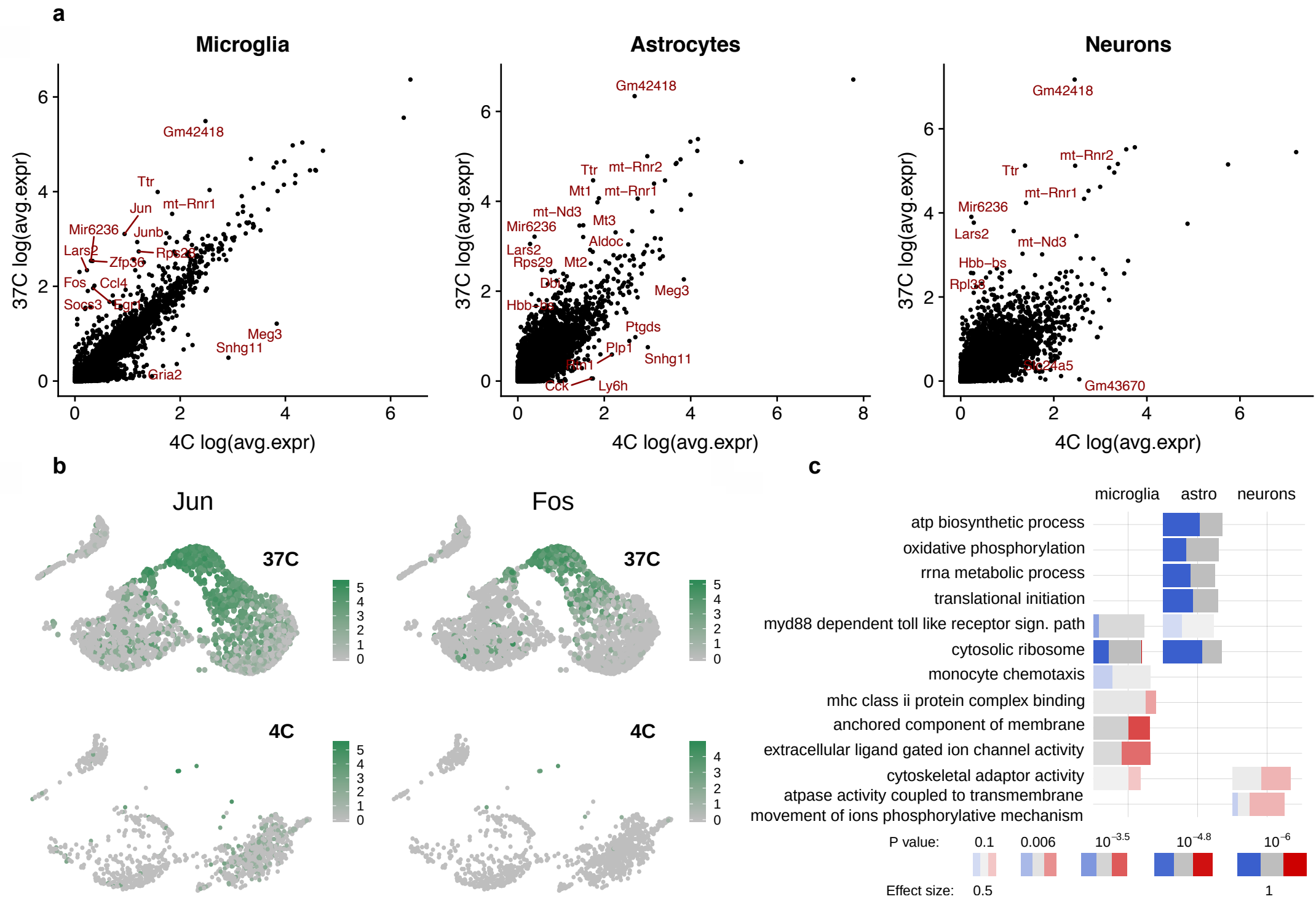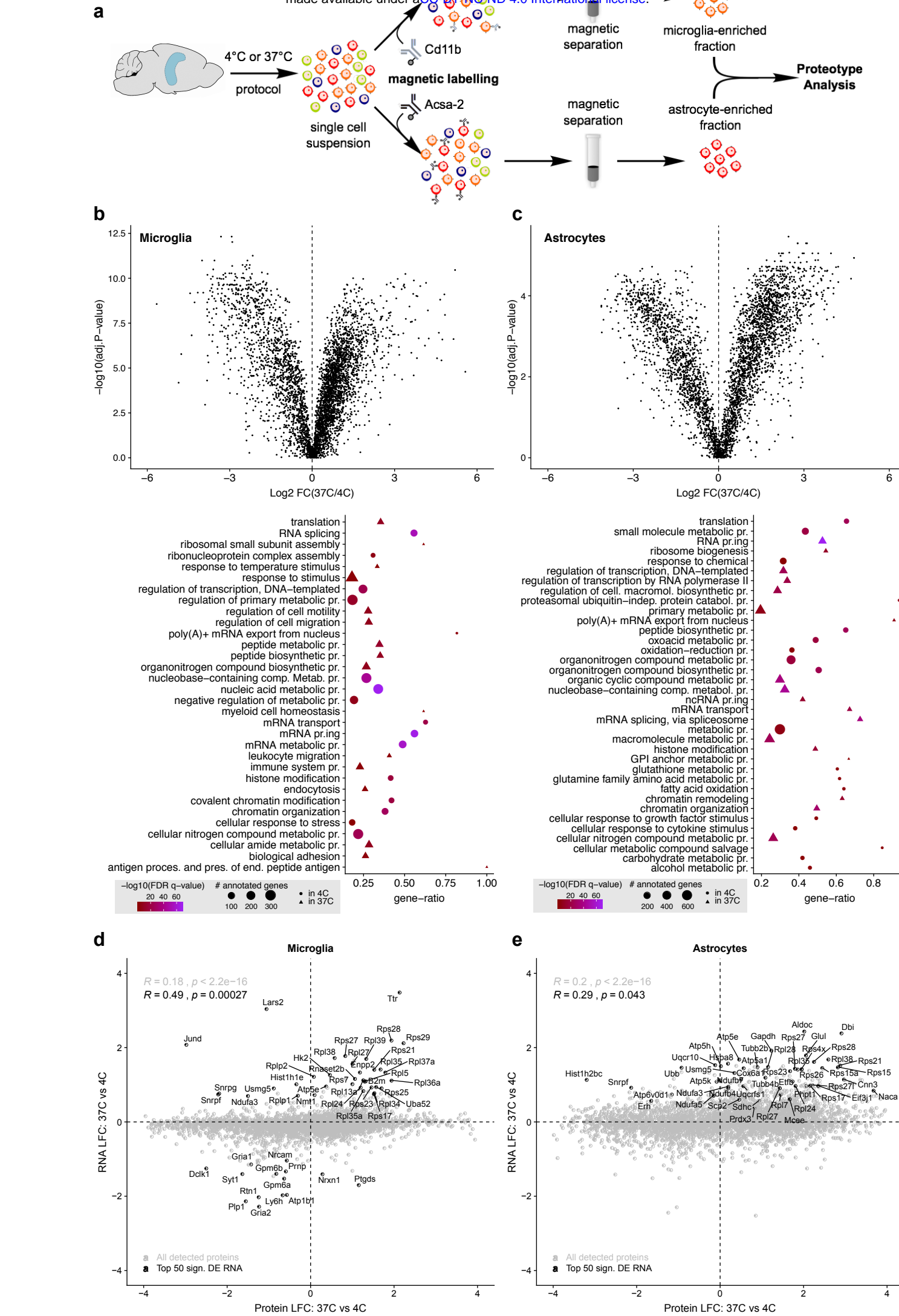
6

Figure 1

Figure 2

Figure 3

Figure 4